Published online 29 June 2020

NAR Cancer, 2020, Vol. 2, No. 2 **1**
doi: 10.1093/narcan/zcaa010

Proteome dynamics analysis identifies functional roles of SDE2 and hypoxia in DNA damage response in prostate cancer cells

Ang Luo[1], Yao Gong[1], Hyungjin Kim[2] and Yue Chen[1,*]

[1]Department of Biochemistry, Molecular Biology and Biophysics, University of Minnesota at Twin Cities, Minneapolis, MN 55455, USA and [2]Department of Pharmacological Sciences, Stony Brook University, Stony Brook, NY 11794, USA

Received February 25, 2020; Revised May 19, 2020; Editorial Decision June 05, 2020; Accepted June 08, 2020

ABSTRACT

Mechanistic understanding of hypoxia-responsive signaling pathways provides important insights into oxygen- and metabolism-dependent cellular phenotypes in diseases. Using SILAC-based quantitative proteomics, we provided a quantitative map identifying over 6300 protein groups in response to hypoxia in prostate cancer cells and identified both canonical and novel cellular networks dynamically regulated under hypoxia. Particularly, we identified SDE2, a DNA stress response modulator, that was significantly downregulated by hypoxia, independent of HIF (hypoxia-inducible factor) transcriptional activity. Mechanistically, hypoxia treatment promoted SDE2 polyubiquitination and degradation. Such regulation is independent of previously identified Arg/N-end rule proteolysis or the ubiquitin E3 ligase, CDT2. Depletion of SDE2 increased cellular sensitivity to DNA damage and inhibited cell proliferation. Interestingly, either SDE2 depletion or hypoxia treatment potentiated DNA damage-induced PCNA (proliferating cell nuclear antigen) monoubiquitination, a key step for translesion DNA synthesis. Furthermore, knockdown of SDE2 desensitized, while overexpression of SDE2 protected the hypoxia-mediated regulation of PCNA monoubiquitination upon DNA damage. Taken together, our quantitative proteomics and biochemical study revealed diverse hypoxia-responsive pathways that strongly associated with prostate cancer tumorigenesis and identified the functional roles of SDE2 and hypoxia in regulating DNA damage-induced PCNA monoubiquitination, suggesting a possible link between hypoxic microenvironment and the activation of error-prone DNA repair pathway in tumor cells.

INTRODUCTION

Aerobic respiration is a highly efficient pathway for energy production in metazoan cells. The process requires oxygen consumption to enable the oxidation of carbons in nutrients and drive the electron transport chain in mitochondria for ATP synthesis that powers diverse cellular processes. Hence, a relatively stable level of oxygen is necessary for energy production and functional maintenance during proliferation and development in cells. Some physiological and pathological conditions, such as embryonic development and tumorigenesis, however, result in a hypoxic microenvironment in tissues. The decrease of oxygen concentration in cellular microenvironment reprograms metabolic networks and contributes to the selection of aerobic fermentation phenotype commonly observed in aggressive cancer cells (1–4). During tumorigenesis, adaptation to hypoxia leads to aggressive cancer phenotypes by promoting genomic instability, tissue invasion, evasion of apoptosis and immune surveillance, as well as the stimulation of cell proliferation and angiogenesis. Therefore, targeting hypoxia response cellular networks has been considered as a viable strategy to develop efficient cancer therapeutics (5,6).

In mammalian cells, extensive studies have established the significance of hypoxic response pathways orchestrated by hypoxia-inducible factors (HIFs) (1–4). Hypoxia microenvironment stabilizes HIF-α factors and promotes the binding of HIF complex to the promoters of their target genes for the induction of gene expression (7). System-wide identification and functional characterization of hypoxia-responsive genes are important to understand how hypoxia regulates cell phenotype and metabolic pathways. Global identification of hypoxia response networks has been largely achieved through genomics and transcriptomics analysis. Hundreds of hypoxia-responsible genes have been identified, including both upregulated and downregulated elements (8–10). These studies mainly applied genomic approaches such as DNA microarray, transcriptome analysis and chromatin immunoprecipitation followed by NextGen

*To whom correspondence should be addressed. Tel: +1 612 626 3340; Email: yuechen@umn.edu

sequencing. The findings from these studies demonstrated the significant roles of HIF transcriptional networks in mediating cellular hypoxia response in cell lines and tissues (1).

In addition to transcription regulation and changes, protein abundance in cells is regulated through multiple mechanisms, including translational control, chemical modification, proteolytic cleavage and protein degradation. Therefore, a system-wide understanding of cellular hypoxia response networks requires the direct measurement of cellular proteome dynamics in response to the hypoxic microenvironment. Recent advances in quantitative proteomics have allowed system-wide identification of hundreds to thousands of proteins and analyze their dynamics under different conditions. Application of such strategies has made important discoveries in hypoxia research, including the recent identification of heterochromatin protein 1 binding protein 3 in tumorigenesis and PHD finger protein 14 in cell cycle control (11–15).

In prostate cancer, tumor tissues suffer from severe hypoxia with the median level of oxygen 13 times lower than the normal prostate tissue (16,17). Activation of hypoxia-induced signaling mechanisms alters the cellular metabolic pathways and energy homeostasis to enable the early development of aggressive cancer phenotype and the adaptation of prostate cancer cells to the hypoxic tissue environment (18,19). Targeting hypoxia-related cellular mechanisms has been considered as a viable strategy for prostate cancer treatment (20,21). To comprehensively understand and system-wide profile proteome dynamics in response to hypoxia in prostate cancer cells, we performed SILAC-based deep proteomic analysis in combination with an efficient high-pH reversed-phase high-performance liquid chromatography (HPLC) fractionation. Our study identified over 6300 protein groups (representing >10 000 leading proteins) in biological triplicate analysis from DU145 cells. Bioinformatic analysis revealed protein networks and complexes highly responsive to early hypoxic treatment and closely linked hypoxia microenvironment to cancer-promoting cellular pathways. Our global proteomic study identified SDE2, a DNA replication and damage-related protein, as a novel cellular target of hypoxia that is rapidly degraded in response to the decrease in oxygen availability (22,23). The functional analysis demonstrated that both hypoxia treatment and depletion of SDE2 can mediate PCNA (proliferating cell nuclear antigen) monoubiquitination upon DNA damage in prostate cancer cells, which is a key step for promoting translesion DNA synthesis. Our study therefore indicated a potential link between hypoxic environment and the activation of error-prone DNA repair pathways in tumor cells.

MATERIALS AND METHODS

Cell lines and reagents

DU145 and PC3 prostate cancer cell lines were cultured in RPMI 1640 medium (Gibco) supplemented with 10% fetal bovine serum (FBS; Sigma) and 1% penicillin–streptomycin (Corning). HeLa and 293T cell lines were cultured in Dulbecco's modified Eagle's medium (Gibco) supplemented with 10% FBS (Sigma) and penicillin–streptomycin (Corning). For SILAC labeling, the DU145 cells were maintained in RPMI 1640 medium for SILAC (Thermo), which was supplemented with 10% dialyzed FBS (Gibco), 1% penicillin–streptomycin, 25 mg/500 ml proline, and 50 mg/500 ml L-arginine and L-lysine (light) or $^{13}C_6{}^{15}N_4$-L-arginine and $^{13}C_6{}^{15}N_2$-L-lysine (heavy). The cells were labeled, respectively, in the light and heavy media for >6 generations before doing a further treatment. For hypoxia treatment, the cells were cultured in an incubator subchamber supplied with 1% O_2/5% CO_2/95% N_2 and monitored by an oxygen sensor (BioSperix). The main chemicals used in this study included puromycin (EMD Millipore), MG132 (APExBIO), dimethyloxalylglycine (DMOG; APExBIO) and deferoxamine (DFO; Cayman).

Mass spectrometry sample preparation

Twenty-four hours after plating, the heavy-labeled Du145 cells were transferred into a hypoxia chamber (1% O_2), while the light-labeled cells were still kept at normal culture condition (21% O_2). Twelve hours after hypoxia treatment, the cells were washed with phosphate-buffered saline (PBS) and lysed in boiling denatured lysis buffer (6 M guanidine hydrochloride in 50 mM Tris–HCl, pH 8.5). The cell lysates were further boiled in boiling water for 5 min, cooled to room temperature (RT) and then sonicated thoroughly. After protein concentration measurement with the Bradford assay (Thermo), equal amounts of heavy- and light-labeled proteins were mixed. The mixed proteins were reduced and alkylated simultaneously in 5 mM tris(2-carboxyethyl)phosphine hydrochloride/10 mM iodoacetamide at RT for 1 h in the dark. For enzymatic digestion, the proteins were first treated with Lys-C (1:100; Wako) for 5 h at 37°C, and then the lysates were diluted with 50 mM Tris–HCl for four times and further digested with trypsin (1:100; Promega) overnight at 37°C. The digestion product was centrifuged at 2000 × *g* for 10 min and the supernatant was desalted with a Sep-Pak C18 cartridge (100 mg, Waters) and eluted with 50% acetonitrile (ACN). The elution was dried in a speed vacuum to prepare for fractionation.

Basic reversed-phase HPLC offline fractionation

Desalted peptide solution was loaded onto an XBridge Peptide BEH C18 column (Waters) through an Agilent 1100 HPLC system. The mobile phase is composed of Buffer A, which is 10 mM ammonium formate (pH 10.0), and Buffer B, which is 90% ACN/10 mM ammonium formate (pH 10.0). Peptides were separated with a 60-min fractionation gradient (6–35% B in 43 min and then remaining at 95% B for 12 min) and a flow rate of 1 ml/min. For each sample, all the fractions were pooled in a concatenated manner into eight final fractions as described previously (24).

Nano-HPLC–mass spectrometry analysis

Peptides were desalted with a self-packed C18 StageTip (25). For liquid chromatography–tandem mass spectrometry (LC–MS/MS) analysis, the peptides were dissolved in HPLC buffer A (0.1% formic acid) and loaded onto a capillary HPLC column (25 cm in length, 360 μm outer diameter

and 75 μm inner diameter) packed with ReproSil-Pur Basic C18 resin (1.9 μm particle size and 100 Å pore size) with a Proxeon Easy nLC 1000 Nano-UPLC system connected to an Orbitrap Fusion mass spectrometer (Thermo Fisher). The peptides were eluted off the column with a 1-h gradient of 7–32% HPLC buffer B (0.1% formic acid in ACN). The full MS was acquired with a mass range of 300–1500 m/z at 60 000 resolution (200 m/z). Data-dependent MS/MS spectra were acquired in the ion trap and in a top-speed mode (3 s for each cycle) with an isolation window of 1.6 m/z and higher energy collision dissociation (35% collision energy).

Plasmids, siRNAs and transfection

pcDNA-SDE2-Flag, pcDNA-SDE2-GG/AA-Flag and pcDNA-SDE2-K/V-Flag were plasmids used in our previous studies (22,26). Plasmid transfection was performed with jetPRIME® transfection reagents. Sequences for control siRNA and siRNAs targeting SDE2, CDT2, UBR1 and UBR2 were synthesized by Dharmacon (Lafayette, CO) based on previous publications (22,26–27). HIF1α and HIF2α siRNAs were ordered from Qiagen (Germantown, MD). siRNA transfections were performed with INTERFERin® siRNA and miRNA transfection reagent (Polyplus, Illkirch, France) according to the manufacturer's instructions. All siRNA sequences are listed in Supplementary Table S3.

shRNA and lentivirus packaging

Control shRNA plasmid expressing a scramble sequence was ordered from the Genomics Center of the University of Minnesota. shRNA plasmids targeting SDE2 (TRCN0000370430 and TRCN0000377549) were ordered from Sigma. To establish the stable cell lines, shRNA plasmids were co-transfected into 293FT cells together with psPAX2 and pMD2.G at the ratio of 4:3:1. Forty-eight hours after transfection, the cell medium containing the lentivirus was filtered and used to infect the target cells with the help of polybrene (8 μg/ml). Twenty-four hours after infection, the cells were transferred into medium containing 2 μg/ml puromycin.

Western blotting analysis

The cell lysate was prepared in ice-cold RIPA buffer [150 mM NaCl, 50 mM Tris–HCl, pH 7.5, 0.1% sodium dodecyl sulfate (SDS), 0.5% NP-40 and 0.5% sodium deoxycholate; cocktail protease inhibitor (Roche) was freshly added]. The proteins were separated in homemade SDS-PAGE gel and transferred onto polyvinylidene difluoride membrane. Blocking was done with 5% skim milk (BD) in TBST (Tris-buffered saline + 0.1% Tween 20). After blocking, the membrane was incubated with primary antibody overnight and washed with TBST for at least three times, and then incubated with horseradish peroxidase (HRP)-linked secondary antibody (Cell Signaling Technology, #7074 and #7076) for >2 h and washed with TBST. The signal was developed with Luminata Crescendo Western HRP Substrate (Millipore) and captured on X-ray film. Primary antibodies used in the current study included SDE2 (A302-098A, Bethyl), CDT2 (A300-948A, Bethyl), UBR1 (A302-988A, Bethyl), UBR2 (A305-416A, Bethyl), DDX41 (A302-098A, Bethyl), WDR45B (NBP1-82387, Novus), HIF1α (04-1006, Millipore), HIF1α (SAB2702132, Sigma), HIF2α (A700-003, Bethyl), HIF1β (A302-764A-T, Bethyl), γH2AX (A700-003, Bethyl), ubiquitin (MAB1510, Millipore), PCNA (2586T, Cell Signaling Technology), α-tubulin (T6199, Sigma) and β-actin (3700s, Cell Signaling Technology).

In vivo ubiquitination assay

Two 60-mm dishes of 293T cells were transfected with SDE2-Flag plasmid for 12 h and then treated with 5 μM MG132. One dish of cells was continually cultured under normal conditions, while the other dish was treated with hypoxia for another 12 h. After treatment, the cells were collected in PBS, pelleted and washed with PBS again and resuspended in SDS lysis buffer (150 mM NaCl, 1% SDS, 50 mM Tris–HCl, pH 7.5) and boiled for 10 min. The cell lysate was cooled to room temperature and diluted with dilution buffer (150 mM NaCl, 50 mM Tris–HCl, pH 7.5) to reduce the concentration of SDS to 0.2%, sonicated thoroughly and then centrifuged at 21 000 × g. Ten percent of the supernatant was reserved as the input and the rest was incubated with Flag-M2 beads overnight at 4°C. Finally, the M2 beads were washed with wash buffer (150 mM NaCl, 0.2% SDS, 50 mM Tris–HCl, pH 7.5) for four times and eluted with 1× SDS-PAGE sample loading buffer by boiling for 6 min. The input was mixed with a 4× loading buffer and boiled. The samples were analyzed with western blotting (WB).

Quantitative real-time PCR

Total RNA was isolated from cells using TRIzol Reagent (Ambion) according to the manufacturer's instructions. For each sample, 2 μg raw RNA was reverse transcribed into cDNA with M-MLV Reverse Transcriptase (Promega) in a 25 μl reaction system. The reverse transcription product was further diluted to 150 μl. Two microliters were used as a template for each quantitative real-time PCR (qRT-PCR) reaction. The reaction was performed on CFX96 Touch™ Real-Time PCR Detection System (BioRad) using Luna® Universal qPCR Master Mix (New England Biolabs, M3003). Peptidylprolyl isomerase A was used as the reference gene for normalization. All reactions were run in triplicate. The primers for qRT-PCR are listed in the Supplementary Data (Supplementary Table S4).

Cell viability assay

Cells were seeded in 24-well or 48-well plates at densities between 10^4 and 2×10^4 cells per well, fixed at various time points in 10% trichloroacetic acid at 4°C for 1 h, washed with tap water five times and then dried at the RT. The fixed cells were stained with 0.04% sulforhodamine B (SRB), washed with 1% acetic acid and then dried at RT. Cell-bound SRB was then dissolved in 10 mM Tris–HCl (pH 10), and the optical density was measured with a spectrometer at an absorbing wavelength of 490 nm.

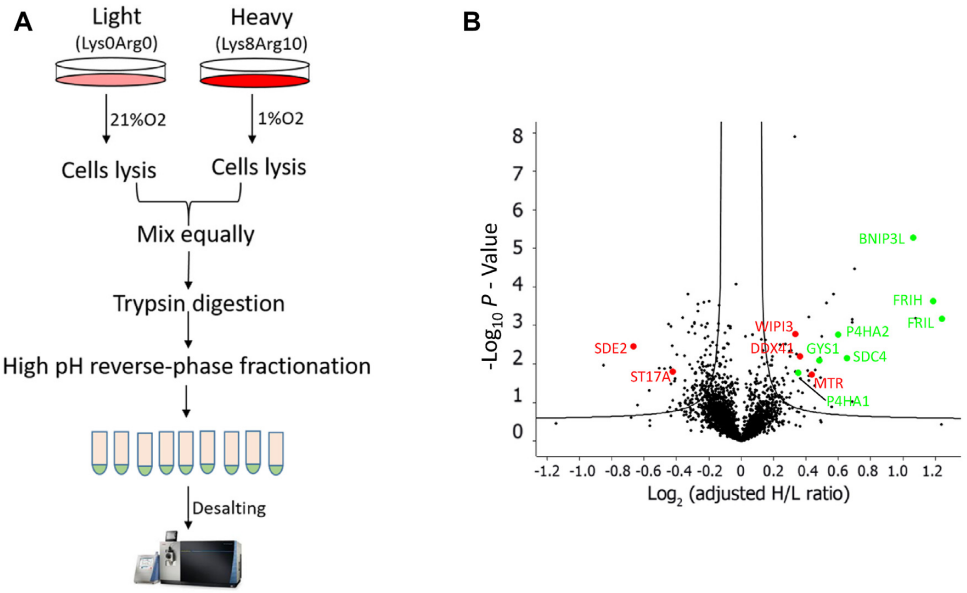

Figure 1. SILAC-based quantitative analysis of proteins regulated by hypoxia in prostate cancer cells. (**A**) A schematic representation of SILAC-based proteomics analysis strategies. (**B**) Volcano plot showing the proteins significantly regulated by hypoxia treatment. Known hypoxia-regulated proteins are colored in green and proteins that were previously unknown to be regulated by hypoxia are colored in red.

Proteome dynamic and bioinformatic analysis

The MS raw data were analyzed with MaxQuant software version 1.5.2.8 (15) and searched against the UniProt human database (73 928 sequences, downloaded on 15 March 2019) with the specification of SILAC amino acid labeling for lysine and arginine. Met oxidation and protein N-terminal acetylation were specified as variable modifications. Cys carbamidomethylation was specified as a fixed modification. Trypsin was specified as the protease with a maximum of two missing cleavages. Bioinformatic analysis was performed with a data processing pipeline in Perseus (28). Briefly, protein SILAC ratios were $\log_2$ transformed and subjected to Student's *t*-test. The $\log_2$ transformed fold changes of proteins in abundance were then plotted in the volcano plot. Proteins that were significantly up- or down-regulated, as well as proteins whose abundance did not show significant changes upon the treatment, were divided into three clusters. Proteins in each cluster were analyzed for functional enrichment in different categories using the total identified proteins in our analysis as the background with the GOstats package in R (29). The *P*-values of the functional annotations in each cluster were $-\log_{10}$ transformed and subject to *z*-score conversion. Functional annotations with significant enrichment in at least one cluster were collected for hierarchical clustering and heat map analysis using Genesis software (30).

Protein subnetwork analysis was performed by extracting highly confident protein–protein interactions (score >700) from the STRING protein interaction database (31) based on all quantifiable proteins in our analysis. From this large network, we performed MCODE analysis to identify subnetworks with high connectivity (32). The average or median SILAC ratios of each subnetwork protein clusters were collected to select for significantly up- or downregulated protein networks. Protein subnetworks were visualized with Cytoscape (v. 3.7.2) (33).

RESULTS

SILAC-based quantitative analysis reveals proteome dynamics in response to hypoxia

In order to quantitatively analyze the proteins regulated by hypoxia response, we adapted the SILAC-based proteomic strategy. DU145 prostate cancer cell line was labeled with either $^{12}C_6{}^{14}N_4$-L-arginine and $^{12}C_6{}^{14}N_2$-L-lysine (light) or $^{13}C_6{}^{15}N_4$-L-arginine and $^{13}C_6{}^{15}N_2$-L-lysine (heavy). The light-labeled cells were cultured under normoxia (21% O_2), while at the same time the heavy-labeled cells were treated under hypoxia (1% O_2). After 12 h of hypoxia treatment, all the cells were harvested very quickly and lysed in a denaturing buffer. Equal amounts of light- and heavy-labeled cells were mixed and digested by trypsin. Peptides were fractionated through high-pH reversed-phase HPLC followed by nano-HPLC–MS/MS analysis. Three biological replicate analyses were performed to facilitate statistical analysis. Our study identified 6320 protein groups in biological triplicate analysis with >10 000 leading proteins, among which 5768 protein groups were quantifiable (Figure 1A).

Bioinformatic analysis shows hypoxia promoting anti-apoptotic pathways in cancer cells

We established a bioinformatic analysis pipeline to identify cellular networks with statistically significant regulation in response to the hypoxia treatment with three biological replicates (Figure 1B). In our analysis, surprisingly, 12 h of hypoxia treatment at 1% oxygen did not induce significant changes to the overall proteome abundance in prostate can-

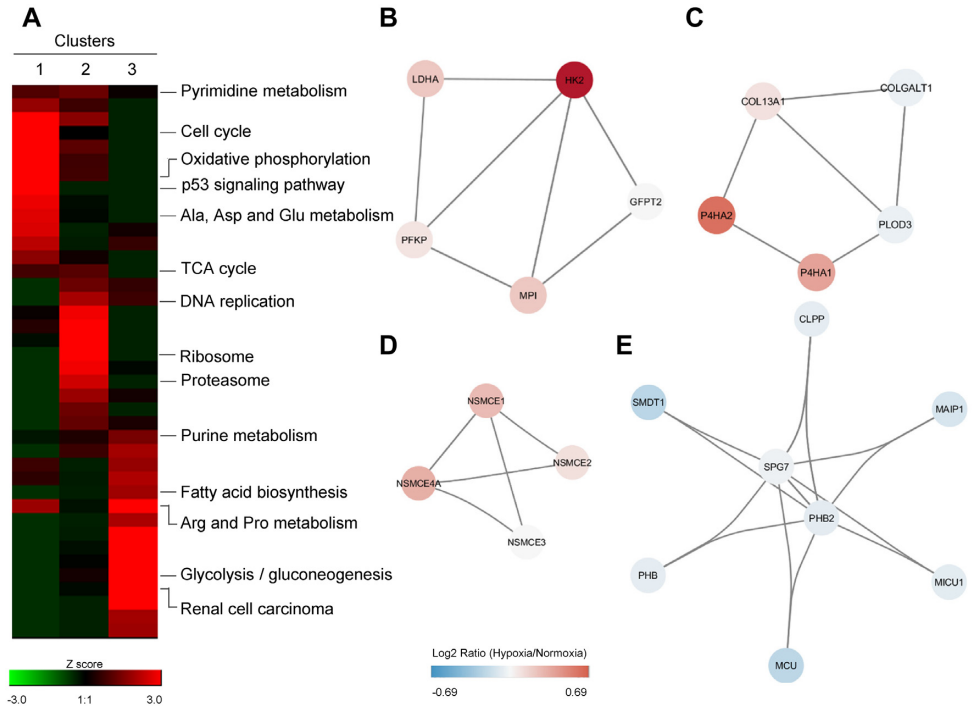

Figure 2. Enrichment and clustering analysis of hypoxic response pathways and networks in prostate cancer cells. (**A**) Heat map representation of enriched KEGG pathways in response to the hypoxia treatment. Quantified proteins in our analysis were grouped into three clusters following significance test, with Cluster 1 representing downregulated proteins, Cluster 3 representing upregulated proteins and Cluster 2 representing proteins whose abundances were not significantly altered. (**B**–**E**) Protein subnetwork quantification analysis. Highly connected protein subnetworks were identified with MCODE. Median or average SILAC ratios (hypoxia/normoxia) of the subnetworks were analyzed to identify protein clusters with significant overall increase or decrease in abundance upon hypoxia treatment.

cer cells. However, analysis of significantly upregulated proteins still identified well-known hypoxia-induced markers, including VEGF, PDK1, P4HA1 and P4HA2. The analysis also identified other proteins, including WDR45B, MTR, OSMR and DDX41, that have not been reported to be induced by hypoxia previously (Figure 1B). Interestingly, we identified a small set of proteins whose abundance decreases under hypoxia and nearly all of them have not been known to be regulated by hypoxia.

To further understand the functional significance of changes, we divided the proteome dataset into three clusters representing proteins that are significantly upregulated, significantly downregulated or not significantly changed in response to the hypoxia treatment (Figure 2A, Supplementary Figure S1). Analysis of pathway and gene ontology in each cluster showed that the metabolic pathways regulating glycolysis and fatty acid biosynthesis were significantly upregulated and the metabolic pathways regulating oxidative phosphorylation and cell cycle were significantly downregulated in prostate cancer cells, which agrees well with known metabolic adaptation to hypoxia (6,34–35). Interestingly, our analysis showed that small molecular metabolisms, including nucleotide and amino acid metabolisms, were differentially regulated in response to hypoxia treatment. Pyrimidine metabolism pathway and Ala, Asp and Glu metabolic pathways were downregulated. On the other hand, the purine metabolism pathway and Arg and Pro metabolic pathways were upregulated. Hypoxia treatment of prostate cancer cells significantly downregulates proteins involved in extracellular matrix-related pathways and expression of cadherin. Such regulation has been known to promote metastasis in different cancers (36). Interestingly, our data showed that pathways related to renal cell carcinoma (RCC) were significantly upregulated upon hypoxia treatment of prostate cancer cells. Previous clinical studies have shown that men with prostate cancer have a significantly higher chance of developing RCC (37). Accordingly, our analysis showed that hypoxia microenvironment in prostate cancer cells significantly upregulated MET and ETS1 to activate key cell proliferation signaling cascades that are important for RCC while upregulating GLUT1 and VEGF to increase nutrient availability, potentially promoting the subsequent development of RCC in prostate cancer patients (38).

To identify the protein networks that were co-regulated in response to hypoxia treatment, we performed a quantitative analysis of interaction subnetwork. Using the MCODE algorithm and STRING protein interaction database, we extracted 106 highly connected protein–protein interaction subnetworks from all proteins identified in our proteomic survey. The average or median SILAC ratios of each cluster were then collected for statistical analysis to identify significantly up- or downregulated protein clusters. Our analysis identified 13 interaction subnetworks that were significantly regulated in prostate cancer cells in response to the hypoxia treatment (Figure 2B, Supplementary Figure S2). As ex-

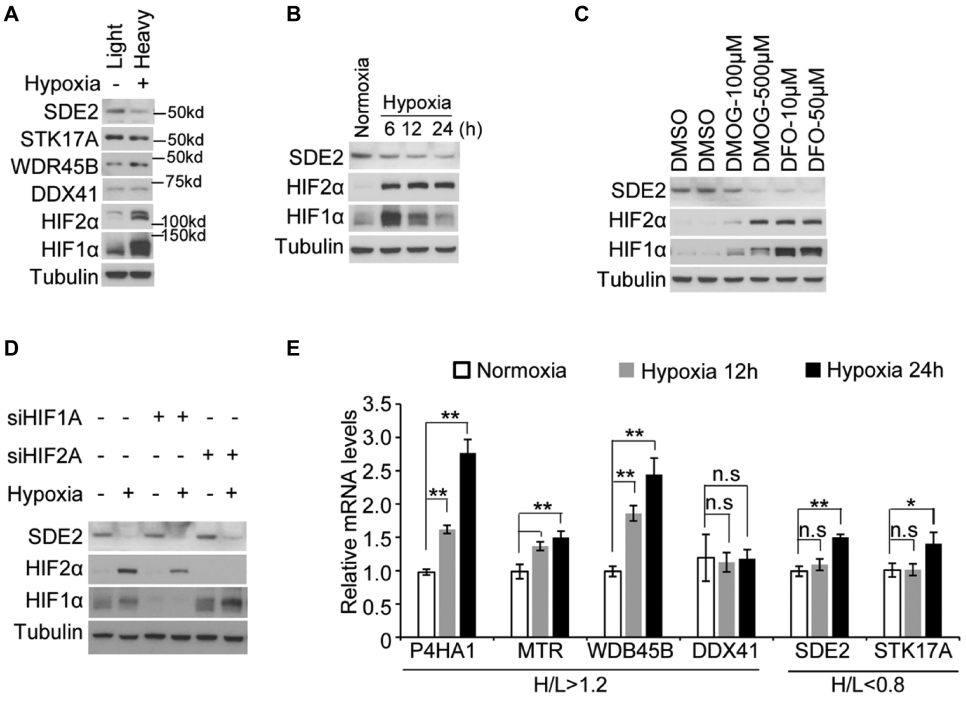

Figure 3. SDE2 is downregulated by hypoxia in DU145 cells. (**A**) WB of whole cell lysates from SILAC-labeled cells that were treated with or without hypoxia for 12 h. (**B**) DU145 cells were treated with or without hypoxia for different times and then prepared for WB with the indicated antibodies. The expression of tubulin served as the loading control. (**C**) DU145 cells were treated with the indicated chemicals for 24 h and then prepared for WB. (**D**) DU145 cells were transfected with the control siRNA or siRNA targeting HIF1α or HIF2α for 24 h, respectively, and then treated with or without hypoxia for another 24 h before being harvested for WB. (**E**) qRT-PCR analysis of the mRNA levels of the indicated genes in DU145 cells treated with or without hypoxia. $^{**}P < 0.01$, $^{*}P < 0.05$, n.s. means not significant. Student's *t*-test, $n = 3$.

pected, our analysis identified protein networks related to glycolysis (involving HK2, LDHA and PFKP) and collagen processing (involving P4HA1, P4HA2 and COL13A1) were upregulated under hypoxia (Figure 2B and C). One significantly upregulated subnetwork identified in our analysis was DNA damage-related E3 ubiquitin-protein cluster (involving NSMCE1, NSMCE2 and NSMCE4A; Figure 2D). The upregulation of the E3 ubiquitin ligase has been known to induce the degradation of MMS19 and impair the activation of DNA repair capacity in cancer cells (39). Therefore, our analysis provided evidence to suggest that hypoxia microenvironment is a contributing factor that promotes DNA instability in prostate cancer cells by upregulating NSMCE1-related E3 ubiquitin ligases and inhibiting efficient DNA repair. In addition to the subnetworks that were significantly upregulated upon the hypoxia treatment, we also identified several downregulated subnetworks. One example is a protein network with mitochondria calcium transporter (involving MCU, SMDT1 and MAIP1). Calcium flux signaling in mitochondria has been known to induce reactive oxygen species and cell apoptosis (40). Previous studies have shown that cancer cells tend to downregulate mitochondria calcium transporter to inhibit cell apoptosis (41,42). Therefore, our analysis suggests that by downregulating mitochondria calcium transporter networks and inhibiting apoptosis, hypoxia environment promotes prostate cancer cell survival under a stressful condition.

Hypoxia treatment reduces the abundance of SDE2 at the protein level

From the lists of proteins that are significantly up- or downregulated in response to hypoxia treatment in prostate cancer cells, we selected a few proteins that are related to tumorigenesis but are not known to be regulated by hypoxia and performed WB for validation in DU145 cells, including WDR45B, DDX41, STK17A and SDE2. The expressions of HIF1α and HIF2α were examined as positive controls for hypoxia treatment. We were able to confirm that hypoxia treatment significantly upregulated WDR45B, while the level of changes for DDX41 was modest (Figure 3A). We also confirmed that the protein levels of STK17A and SDE2 were both reduced under hypoxia (Figure 3A).

Hypoxia-mediated transcriptional activation of over 100 genes by HIF transcription factors has been widely studied, while less is known about proteins decreasing in abundance in response to hypoxia. In this study, we further analyzed SDE2 to understand the mechanism and functional significance of its downregulation under hypoxia. *SDE2* (Silencing Defective 2) gene was first identified in fission yeast recently when the strain lacking this gene was defective in telomere silencing (43). The human *SDE2* is a homolog of *SDE2* in yeast and is conserved between species, especially the SDE domain (Supplementary Figure S3A) (22). On the N-terminal of SDE2, there is a ubiquitin-like (UBL) do-

main, which ranges from 1 to 78 amino acids and has been reported to be cleaved by an unknown deubiquitinating enzyme (DUB) and produce a 50-kDa C-terminal SDE2 in multiple cell lines (22). As expected, the SDE2 protein we detected by WB in the SILAC-labeled DU145 cells was also found at the 50-kDa position (Figure 2A). Our identification and quantification of SDE2 were confident with eight peptides and ∼26% sequence coverage. All the identified peptides were localized outside of the UBL domain (Supplementary Figure S3B).

To further confirm the regulation of hypoxia on SDE2 protein, we first aimed to understand the dynamics of SDE2 in response to different durations of hypoxia treatment. To this end, DU145 cells were treated with hypoxia (1% oxygen) for 6, 12 and 24 h. The WB analysis showed that with the increasing treatment of hypoxia, HIF1α was significantly induced at 6 h and then its abundance gradually decreased after 12 and 24 h of treatment, while the level of HIF2α was induced from the beginning and remained at a high level. In contrast, SDE2 protein showed an apparent decrease in abundance initially and its abundance continued to decrease throughout the treatment (Figure 3B). We further tested whether hypoxia-mimicking drugs can induce a similar effect. To this end, DU145 cells were treated by DMOG, an alpha-ketoglutarate mimic compound, and DFO, an iron chelator, for 24 h. Our data confirmed that both drugs increased the abundances of HIF1α and HIF2α, and reduced the protein level of SDE2, in a dosage-dependent manner (Figure 3C). These data suggested that hypoxia-mediated regulation of SDE2 protein abundance requires enzymatic activities of alpha-ketoglutarate and iron-dependent proteins.

Because HIF1α and HIF2α are master regulators of hypoxia response, next we tested whether the regulation of hypoxia on SDE2 requires HIF transcriptional activity. To this end, we performed siRNA knockdown experiments. We found that knockdown of HIF1α and HIF2α was effective in DU145 cells, but their knockdown did not affect the hypoxia-dependent decrease in SDE2 abundance (Figure 3D). In addition, in DU145 cells with HIF1β knockdown, hypoxia can still reduce the level SDE2 protein (Supplementary Figure S4). Finally, we tested whether the regulation of hypoxia on SDE2 happened at the transcriptional level. We performed qRT-PCR to measure the relative mRNA level of *SDE2* in DU145 cells treated with different durations of hypoxia. As a control, we also measured the mRNA of several other proteins quantified in our proteomic analysis. Our data showed that hypoxia treatment significantly increased the mRNA level of *P4HA1*, which is a known HIF1α target that showed a significant increase in abundance in our data. For *MTR* and *WDR45B* genes, whose protein levels showed a significant increase in the proteomic analysis, their expression was also significantly induced upon hypoxia (Figure 3E). Interestingly, the mRNA levels of *STK17A* and *SDE2*, the two genes whose protein levels showed a significant decrease in abundance, were not affected by hypoxia after 12 h of treatment and even increased after 24 h of treatment (Figure 3E). Our data suggested that the hypoxic microenvironment regulated SDE2 protein abundance likely through the regulation of its protein degradation rather than at the transcriptional level.

Hypoxia treatment increases the ubiquitination of SDE2 and promotes proteasome-mediated degradation

As our previous studies showed that ultraviolet (UV) treatment decreased the protein level of SDE2 by increasing SDE2 ubiquitination, we sought to test whether hypoxia treatment mediates SDE2 degradation through similar pathways. First, we found that in DU145 cells, the decrease of SDE2 protein abundance under hypoxia was completely blocked by proteasome inhibitor MG132. We further confirmed this observation in HeLa cells where we also confirmed that the mRNA level of *SDE2* was not decreased under hypoxia (Figure 4A, Supplementary Figure S5C and D). Proteasome inhibition also inhibited the SDE2 degradation in prostate cancer cell PC3. However, we found that the *SDE2* mRNA level was reduced in PC3 cells upon hypoxia treatment, suggesting the SDE2 protein level was also regulated at the transcriptional level in PC3 cells (Supplementary Figure S5A and B). Next, we performed immunoprecipitation and WB analysis to detect ubiquitination level changes of SDE2 in DU145 cells upon treatment. Our data showed that hypoxia significantly increased the ubiquitination level of SDE2 (Figure 4B). This was also confirmed in 293T cells (Figure 4C and D).

Three ubiquitin E3 ligases, including CDT2, UBR1 and UBR2, have been reported to regulate the ubiquitination and degradation of SDE2 under UV treatment (22,26). The degradation of SDE2 by CDT2 depends on the cleavage of the N-terminal UBL domain where the last two amino acids are Gly(76)–Gly(77). After cleavage of the UBL domain, the lysine residue exposed as the first amino acid of the C-terminal SDE2 was necessary for the recognition and degradation by UBR1 and UBR2. Since SDE2 was degraded under hypoxia, we wonder whether similar pathways mediate SDE2 degradation. To this end, 293T cells were transfected with Flag-tagged plasmids expressing WT or mutant (GG to AA or K to V) SDE2, respectively. Twelve hours after transfection, the cells were treated with or without hypoxia for 12 h. WB showed that mutation of GG linker amino acids at the C-terminus of the UBL domain or mutation of the first lysine following the GG linker did not affect the degradation of SDE2 in response to hypoxia treatment, suggesting that different mechanisms are involved in the process (Figure 4E and F). This conclusion is further strengthened in 293T cells where SDE2 was still degraded upon hypoxia treatment when CDT2 was knocked down (Figure 4G). Moreover, in both DU145 cells and HeLa cells, knockdown of any of the E3 ligases (CDT2, UBR1 and UBR2) could not affect the SDE2 degradation in response to the hypoxia treatment, indicating other unknown E3 ligases may be involved (Supplementary Figure S4E and F). Surprisingly in HeLa cells, the abundance of UBR2 and CDT2 even decreased upon hypoxia treatment, further suggesting that the known E3 ligases are not involved in the regulation of hypoxia-mediated degradation of SDE2 (Supplementary Figure S5E).

Knockdown of SDE2 inhibits cell proliferation and increases DNA damage

Our previous studies showed that SDE2 plays an important role in the DNA damage response in HeLa cells and U2OS

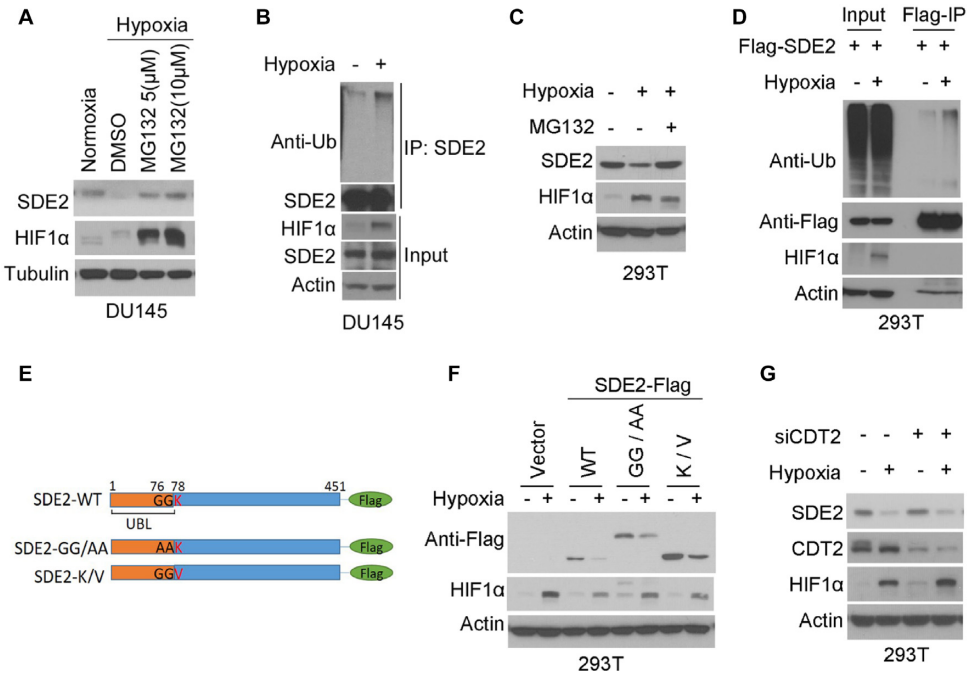

Figure 4. Hypoxia treatment mediated ubiquitination and proteasome-dependent degradation of SDE2. (**A**) DU145 cells were treated with hypoxia for 16 h and then DMSO or MG132 was added for another 8 h. The cells were prepared for WB 24 h after hypoxia treatment. (**B**) DU145 cells were treated with or without hypoxia for 12 h and then treated with 5 μM MG132 for another 12 h. The cells were then harvested for immunoprecipitation with SDE2 antibody and then WB was performed with the indicated primary antibodies. (**C**) 293T cells were exposed to the indicated conditions for 12 h and then harvested for WB. (**D**) 293T cells were transfected with SDE2-Flag plasmid for 12 h and then treated with 5 μM MG132 and with or without hypoxia for another 12 h. The cells were harvested for immunoprecipitation with Flag-M2 beads and then WB was performed with the indicated antibodies. (**E**) Schematic representations of wild-type (WT) and site-specific mutant plasmids of SDE2. (**F**) 293T cells were transfected with the indicated plasmids for 12 h and then exposed to hypoxia or not for another 12 h. After treatment, the cells were collected for WB with the indicated antibodies. (**G**) 293T cells were transfected with control siRNA or siRNA targeting CDT2 for 24 h and then exposed to hypoxia or not for another 24 h. After treatment, the cells were collected for WB with the indicated antibodies.

cells. Here, we would like to confirm that it mediates similar pathways in prostate cancer cells. Interestingly, knockdown of SDE2 by shRNAs inhibited the growth of DU145 cells under both normoxia and hypoxia conditions (Figure 5A and B). This means SDE2 plays some essential roles in cell survival. Similar to HeLa cells, knockdown of SDE2 increased the sensitivity of DU145 cells to the DNA damage drug hydroxyurea (HU), an effect that was further verified by the increased level of γH2AX (Figure 5C and D).

SDE2 regulates PCNA monoubiquitination in an oxygen-dependent manner

Monoubiquitination of PCNA promotes the activation of translesion DNA synthesis through recruiting error-prone DNA polymerases (44). Our previous studies have shown that the knockdown of SDE2 enhances the induction of PCNA monoubiquitination upon DNA damage, thus activating error-prone DNA damage repair pathways (22). As we found that SDE2 quickly degrades in response to the hypoxia treatment, we would like to determine whether the hypoxia-mediated degradation of SDE2 also regulates PCNA monoubiquitination. To this end, we performed the dose-dependent treatment of DU145 cells with HU under hypoxia or normoxia. Indeed, increasing concentration of HU treatment resulted in an increased level of PCNA monoubiquitination under normoxia (Supplementary Figure S6). Hypoxia alone without HU treatment did not apparently induce PCNA monoubiquitination. Under the hypoxic environment, SDE2 was degraded and the HU treatment resulted in a much more significant increase of PCNA monoubiquitination in a dose-dependent manner (Supplementary Figure S6).

To determine the mechanistic role of SDE2 in hypoxia-dependent regulation of PCNA monoubiquitination upon DNA damage, we performed SDE2 knockdown studies. Our analysis showed that knockdown of SDE2 in DU145 cells under normoxia led to an increased level of PCNA monoubiquitination upon HU treatment, which agreed well with our previous findings in HeLa cells (22). Hypoxia treatment of control DU145 cells showed similar stimulation of PCNA monoubiquitination upon HU treatment. Interestingly, hypoxia treatment of DU145 cells with SDE2 knockdown did not show a further increase of DNA damage-induced PCNA monoubiquitination (Figure 6A). These data suggested that reduced levels of SDE2 protein desensitize the cells from hypoxia-mediated enhancement of PCNA monoubiquitination under genotoxic stress.

We further performed overexpression experiments in HEK293T cells. Our analysis showed that overexpression of SDE2 under normoxia was sufficient to inhibit the activation of PCNA monoubiquitination upon DNA damage. However, SDE2 overexpression under hypoxia failed to regulate the level of DNA damage-induced PCNA monoubiq-

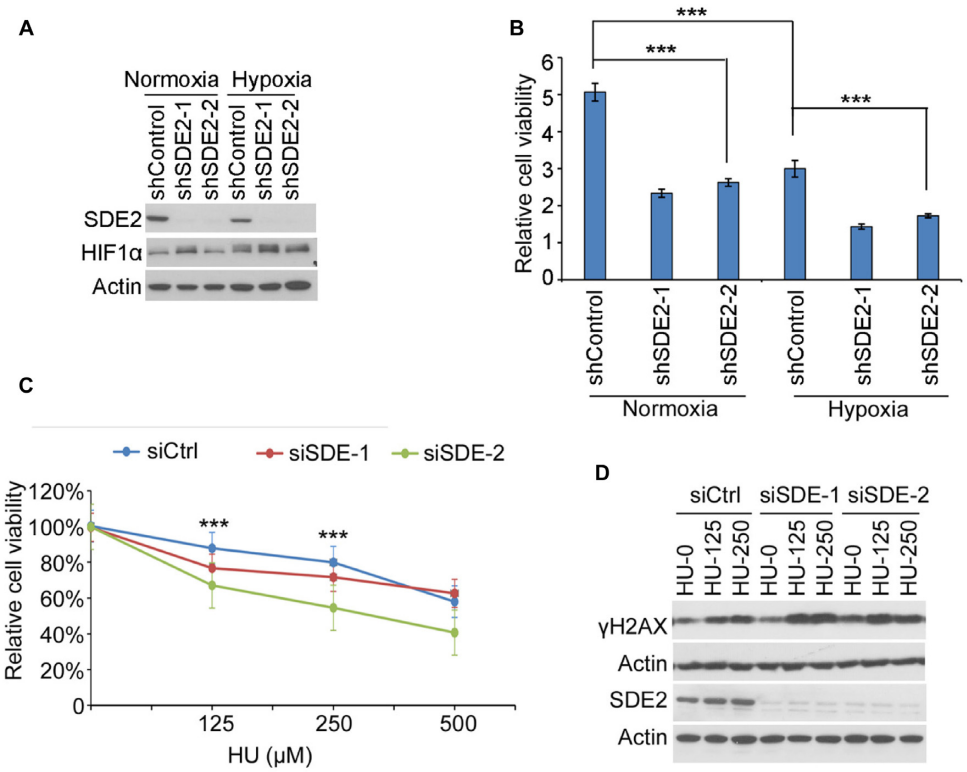

Figure 5. Depletion of SDE2 inhibited cell proliferation and increased DNA damage. (**A**) Verification of SDE2 shRNA knockdown efficiency using WB. (**B**) Cell proliferation under normoxia and hypoxia with SDE2 knockdown. DU145 cells were plated in 24-well plates and then infected with lentivirus expressing control shRNA for SDE2 shRNAs. Twenty-four hours after infection, the cells were started to be cultured in medium containing 2 μg/ml puromycin and treated with or without hypoxia for another 48 h, and then the cells were prepared for the SRB assay to measure the cell viability. (**C**) Cell viability with DNA damage reagent HU treatment. DU145 cells plated and transfected as in (B). Twenty-four hours after transfection, the cells were treated with or without different concentrations of HU for 48 h. Then, the cells were prepared for the SRB assay. For (B) and (C), $***P < 0.001$, $*P < 0.05$. Student's *t*-test, $n = 3$. (**D**) DU145 cells were transfected with the control siRNA (siCtrl) or siRNAs targeting SDE2 (siSDE-1 and siSDE-2) for 24 h and then treated with or without HU for 24 h.

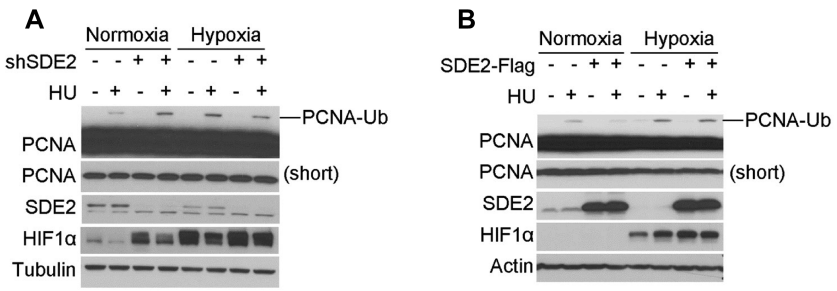

Figure 6. SDE2 regulated PCNA monoubiquitination in an oxygen-dependent manner. (**A**) DU145 cells expressing either control shRNA or shRNA targeting SDE2 were exposed to the indicated conditions for 24 h and then harvested for WB. (**B**) HEK293T cells were transfected with either control vector or SDE2-Flag plasmids. Twelve hours after transfection, the cells were treated with the indicated conditions for another 24 h, and then harvested for WB.

uitination. Cells with SDE2 overexpression showed similar or even greater sensitivity to hypoxia-mediated enhancement of PCNA monoubiquitination in response to HU (Figure 6B). Taken together, our knockdown and overexpression experiments led to these findings. First, SDE2 regulates the DNA damage-induced PCNA monoubiquitination in an oxygen-dependent manner. Second, hypoxia treatment uncouples SDE2 from its regulatory pathways that counteract PCNA monoubiquitination upon DNA damage. Third, SDE2 depletion desensitizes while SDE2 overexpression protects the hypoxia-mediated activation of PCNA monoubiquitination triggered by DNA damage.

DISCUSSION

The tumor microenvironment is critical for tumorigenesis, progression and resistance to drug treatment (45). Hypoxia, as a common feature of the tumor microenvironment, regulates multiple hallmarks of cancer, including but not limited to reprogramming of metabolic pathways, ge-

nomic instability, induction of angiogenesis and evasion of the immune system (46). In the current study, we applied SILAC-based proteomic analysis and used prostate cancer cell line DU145 as a model to profile proteome dynamics in the early response to the hypoxic microenvironment. With three biological replicates and chromatographic fractionations, our deep proteomics analysis identified over 6300 protein groups (representing >10 000 leading proteins), among which 128 protein groups were significantly upregulated and 69 protein groups were significantly downregulated upon hypoxia treatment in prostate cancer cells. Our bioinformatic analysis confirmed well-known hypoxic response pathways (47) and also identified novel protein subnetworks that are highly regulated in a coordinated manner in response to the hypoxia treatment, including DNA damage-related E3 ubiquitin ligases and mitochondria calcium transporter network. Importantly, the upregulation of E3 ligases like NSMCE1 will lead to degradation of key DNA repair proteins and reduce cell's capacity to repair DNAs. Mitochondria calcium transporter activates cell apoptosis by increasing calcium flux to the mitochondria under stress. Hypoxia microenvironment downregulates calcium transporter proteins and therefore inhibits apoptotic cell signaling.

Previous studies have shown that hypoxia downregulated DNA repair proteins, such as RAD51, KU70, RIF1, BRCA1 and BRCA2, and therefore reduced the cellular capacity to repair DNA damage (48,49). In this study, we identified and validated that SDE2, a recently characterized protein that is involved in the DNA damage response pathway, is downregulated by hypoxia. Interestingly, unlike many proteins downregulated under hypoxia due to HIF1α-mediated transcriptional repression, such as apoptosis-inducing factor and antigen-presenting MHC class I molecules (50,51), the degradation of SDE2 under hypoxia is independent of both HIF1α and HIF2α, and in some cases, the mRNA level of *SDE2* was even increased upon hypoxia treatment, suggesting the involvement of critical posttranslational regulation pathways. We were able to confirm that hypoxia degrades SDE2 through the increase of its ubiquitination level and promotes proteasome-dependent protein turnover. Surprisingly, the degradation of SDE2 is independent of CDT2, UBR1 and UBR2, the three ubiquitin E3 ligases that were recently demonstrated to control the stability of SDE2 upon DNA damage (22,26).

SDE2 has been known to associate with PCNA and the loss of SDE2 stimulated PCNA monoubiquitination, which may potentially promote error-prone DNA damage repair. In this study, we found that hypoxia treatment also stimulated DNA damage-induced PCNA monoubiquitination in an SDE2-dependent manner. Loss of SDE2 desensitized while overexpression of SDE2 protected hypoxia-mediated enhancement of PCNA monoubiquitination under the DNA damage response. Indeed, re-analysis of TCGA data (https://www.cancer.gov/tcga) showed that downregulation of SDE2 is prevalent in prostate cancer and it is associated with mutation disease phenotype as well as poorer patient outcome. Analysis with quantitative proteomics experiments also confirmed significantly lower abundance of SDE2 protein in prostate cancer tissue compared to the normal tissue (52). We speculate that low level of SDE2 and hypoxic microenvironment in tissue would contribute to the activation of the error-prone DNA repair pathway and promote cancer cell mutations under both normoxia and hypoxia conditions (53).

In this study, we confirmed that hypoxia mediates the degradation of SDE2 through increasing ubiquitination and proteasome-dependent protein degradation. However, the molecular mechanisms on how and why SDE2 is degraded under hypoxic conditions remain unknown. Our previous studies in HeLa and U2OS cells have shown that degradation of SDE2 requires its endolytic cleavage via the GG linker as well as the exposed N-terminal lysine on the mature protein form. The process is mediated by E3 ubiquitin ligases CDT2, UBR1 and UBR2. However, in prostate cancer cells, we found that hypoxia-mediated degradation of SDE2 does not involve similar pathways. Therefore, additional posttranslational regulatory mechanisms must be required for the rapid degradation of SDE2 under hypoxia. Interestingly, in addition to oxygen level, hypoxia-mimicking drugs, DMOG and DFO, can both recapitulate the effect of hypoxia on SDE2 protein degradation. Given the fact that DMOG is an alpha-ketoglutarate mimic and DFO is an iron chelator, it is likely that SDE2 protein degradation is promoted by alpha-ketoglutarate and iron-dependent enzymes.

Overall, our global analysis of proteome dynamics under hypoxia revealed that hypoxic microenvironment, in addition to reprogramming cellular energy homeostasis and metabolic pathways, may provide an important capability for a tumor cell to survive and evolve under stressful conditions, including genome instability and anti-apoptosis. Potentiation of PCNA monoubiquitination upon DNA damage by hypoxia or by downregulation of SDE2 may potentially exacerbate error-prone DNA repair pathway activation and promote missense mutations for an increased mutational landscape, which play a pathologically critical role in cancer development, drug resistance and phenotypic selection. Further studying hypoxia-dependent regulation of PCNA monoubiquitination and DNA repair pathways by SDE2 may provide new insights and opportunities in cancer therapy.

DATA AVAILABILITY

The MS proteomics data have been deposited to the ProteomeXchange Consortium via the PRIDE (54) partner repository with the dataset identifier PXD017607.

SUPPLEMENTARY DATA

Supplementary Data are available at NAR Cancer Online.

ACKNOWLEDGEMENTS

We are grateful for the discussions and suggestions from the members of the Chen lab during the project development. MS analysis was performed in the Center for Mass Spectrometry and Proteomics, University of Minnesota at Twin Cities. DU145 and PC3 prostate cancer cell lines were kind gifts from Scott Dehm.

FUNDING

National Institutes of Health [R35GM124896 to Y.C., R01CA218132 to H.K.]; American Cancer Society [132235-RSG-18-037-DMC to H.K.].
Conflict of interest statement. None declared.

REFERENCES

1. Semenza,G.L. (2012) Hypoxia-inducible factors in physiology and medicine. *Cell*, **148**, 399–408.
2. Kaelin,W.G. Jr and Ratcliffe,P.J. (2008) Oxygen sensing by metazoans: the central role of the HIF hydroxylase pathway. *Mol. Cell*, **30**, 393–402.
3. Majmundar,A.J., Wong,W.J. and Simon,M.C. (2010) Hypoxia-inducible factors and the response to hypoxic stress. *Mol. Cell*, **40**, 294–309.
4. Dunwoodie,S.L. (2009) The role of hypoxia in development of the mammalian embryo. *Dev. Cell*, **17**, 755–773.
5. Semenza,G.L. (2003) Targeting HIF-1 for cancer therapy. *Nat. Rev. Cancer*, **3**, 721–732.
6. Al Tameemi,W., Dale,T.P., Al-Jumaily,R.M.K. and Forsyth,N.R. (2019) Hypoxia-modified cancer cell metabolism. *Front. Cell Dev. Biol.*, **7**, 4.
7. Dengler,V.L., Galbraith,M. and Espinosa,J.M. (2014) Transcriptional regulation by hypoxia inducible factors. *Crit. Rev. Biochem. Mol. Biol.*, **49**, 1–15.
8. Mole,D.R., Blancher,C., Copley,R.R., Pollard,P.J., Gleadle,J.M., Ragoussis,J. and Ratcliffe,P.J. (2009) Genome-wide association of hypoxia-inducible factor (HIF)-1alpha and HIF-2alpha DNA binding with expression profiling of hypoxia-inducible transcripts. *J. Biol. Chem.*, **284**, 16767–16775.
9. Schodel,J., Oikonomopoulos,S., Ragoussis,J., Pugh,C.W., Ratcliffe,P.J. and Mole,D.R. (2011) High-resolution genome-wide mapping of HIF-binding sites by ChIP-seq. *Blood*, **117**, e207–e217.
10. Chi,J.T., Wang,Z., Nuyten,D.S., Rodriguez,E.H., Schaner,M.E., Salim,A., Wang,Y., Kristensen,G.B., Helland,A., Borresen-Dale,A.L. *et al.* (2006) Gene expression programs in response to hypoxia: cell type specificity and prognostic significance in human cancers. *PLoS Med.*, **3**, e47.
11. Dutta,B., Yan,R., Lim,S.K., Tam,J.P. and Sze,S.K. (2014) Quantitative profiling of chromatome dynamics reveals a novel role for HP1BP3 in hypoxia-induced oncogenesis. *Mol. Cell. Proteomics*, **13**, 3236–3249.
12. Park,J.E., Tse,S.W., Xue,G., Assisi,C., Maqueda,A.S., Ramon,G.P.X., Low,J.K., Kon,O.L., Tay,C.Y., Tam,J.P. *et al.* (2019) Pulsed SILAC-based proteomic analysis unveils hypoxia- and serum starvation-induced *de novo* protein synthesis with PHD finger protein 14 (PHF14) as a hypoxia sensitive epigenetic regulator in cell cycle progression. *Oncotarget*, **10**, 2136–2150.
13. Djidja,M.C., Chang,J., Hadjiprocopis,A., Schmich,F., Sinclair,J., Mrsnik,M., Schoof,E.M., Barker,H.E., Linding,R., Jorgensen,C. *et al.* (2014) Identification of hypoxia-regulated proteins using MALDI-mass spectrometry imaging combined with quantitative proteomics. *J. Proteome Res.*, **13**, 2297–2313.
14. Greenhough,A., Bagley,C., Heesom,K.J., Gurevich,D.B., Gay,D., Bond,M., Collard,T.J., Paraskeva,C., Martin,P., Sansom,O.J. *et al.* (2018) Cancer cell adaptation to hypoxia involves a HIF–GPRC5A–YAP axis. *EMBO Mol. Med.*, **10**, e8699.
15. Cox,J. and Mann,M. (2008) MaxQuant enables high peptide identification rates, individualized p.p.b.-range mass accuracies and proteome-wide protein quantification. *Nat Biotechnol.*, **26**, 1367–1372.
16. Movsas,B., Chapman,J.D., Hanlon,A.L., Horwitz,E.M., Pinover,W.H., Greenberg,R.E., Stobbe,C. and Hanks,G.E. (2001) Hypoxia in human prostate carcinoma: an Eppendorf PO_2 study. *Am. J. Clin. Oncol.*, **24**, 458–461.
17. McKeown,S.R. (2014) Defining normoxia, physoxia and hypoxia in tumours—implications for treatment response. *Br. J. Radiol.*, **87**, 20130676.
18. Bao,B., Ahmad,A., Kong,D., Ali,S., Azmi,A.S., Li,Y., Banerjee,S., Padhye,S. and Sarkar,F.H. (2012) Hypoxia induced aggressiveness of prostate cancer cells is linked with deregulated expression of VEGF, IL-6 and miRNAs that are attenuated by CDF. *PLoS One*, **7**, e43726.
19. Deep,G. and Panigrahi,G.K. (2015) Hypoxia-induced signaling promotes prostate cancer progression: exosomes role as messenger of hypoxic response in tumor microenvironment. *Crit. Rev. Oncog.*, **20**, 419–434.
20. Nesbitt,H., Byrne,N.M., Williams,S.N., Ming,L., Worthington,J., Errington,R.J., Patterson,L.H., Smith,P.J., McKeown,S.R. and McKenna,D.J. (2017) Targeting hypoxic prostate tumors using the novel hypoxia-activated prodrug OCT1002 inhibits expression of genes associated with malignant progression. *Clin. Cancer Res.*, **23**, 1797–1808.
21. Jayaprakash,P., Ai,M., Liu,A., Budhani,P., Bartkowiak,T., Sheng,J., Ager,C., Nicholas,C., Jaiswal,A.R., Sun,Y. *et al.* (2018) Targeted hypoxia reduction restores T cell infiltration and sensitizes prostate cancer to immunotherapy. *J. Clin. Invest.*, **128**, 5137–5149.
22. Jo,U., Cai,W., Wang,J., Kwon,Y., D'Andrea,A.D. and Kim,H. (2016) PCNA-dependent cleavage and degradation of SDE2 regulates response to replication stress. *PLoS Genet.*, **12**, e1006465.
23. Thakran,P., Pandit,P.A., Datta,S., Kolathur,K.K., Pleiss,J.A. and Mishra,S.K. (2018) Sde2 is an intron-specific pre-mRNA splicing regulator activated by ubiquitin-like processing. *EMBO J.*, **37**, 89–101.
24. Yang,F., Shen,Y., Camp,D.G. 2nd and Smith,R.D. (2012) High-pH reversed-phase chromatography with fraction concatenation for 2D proteomic analysis. *Expert Rev. Proteomics*, **9**, 129–134.
25. Rappsilber,J., Mann,M. and Ishihama,Y. (2007) Protocol for micro-purification, enrichment, pre-fractionation and storage of peptides for proteomics using StageTips. *Nat. Protoc.*, **2**, 1896–1906.
26. Rageul,J., Park,J.J., Jo,U., Weinheimer,A.S., Vu,T.T.M. and Kim,H. (2019) Conditional degradation of SDE2 by the Arg/N-end rule pathway regulates stress response at replication forks. *Nucleic Acids Res.*, **47**, 3996–4010.
27. Kannouche,P.L., Wing,J. and Lehmann,A.R. (2004) Interaction of human DNA polymerase eta with monoubiquitinated PCNA: a possible mechanism for the polymerase switch in response to DNA damage. *Mol. Cell*, **14**, 491–500.
28. Tyanova,S. and Cox,J. (2018) Perseus: a bioinformatics platform for integrative analysis of proteomics data in cancer research. *Methods Mol. Biol.*, **1711**, 133–148.
29. Falcon,S. and Gentleman,R. (2007) Using GOstats to test gene lists for GO term association. *Bioinformatics*, **23**, 257–258.
30. Sturn,A., Quackenbush,J. and Trajanoski,Z. (2002) Genesis: cluster analysis of microarray data. *Bioinformatics*, **18**, 207–208.
31. Szklarczyk,D., Gable,A.L., Lyon,D., Junge,A., Wyder,S., Huerta-Cepas,J., Simonovic,M., Doncheva,N.T., Morris,J.H., Bork,P. *et al.* (2019) STRING v11: protein–protein association networks with increased coverage, supporting functional discovery in genome-wide experimental datasets. *Nucleic Acids Res.*, **47**, D607–D613.
32. Bader,G.D. and Hogue,C.W. (2003) An automated method for finding molecular complexes in large protein interaction networks. *BMC Bioinformatics*, **4**, 2.
33. Shannon,P., Markiel,A., Ozier,O., Baliga,N.S., Wang,J.T., Ramage,D., Amin,N., Schwikowski,B. and Ideker,T. (2003) Cytoscape: a software environment for integrated models of biomolecular interaction networks. *Genome Res.*, **13**, 2498–2504.
34. Ortmann,B., Druker,J. and Rocha,S. (2014) Cell cycle progression in response to oxygen levels. *Cell. Mol. Life Sci.*, **71**, 3569–3582.
35. Semenza,G.L. (2011) Hypoxia. Cross talk between oxygen sensing and the cell cycle machinery. *Am. J. Physiol. Cell Physiol.*, **301**, C550–C552.
36. Esteban,M.A., Tran,M.G., Harten,S.K., Hill,P., Castellanos,M.C., Chandra,A., Raval,R., O'Brien,T.S. and Maxwell,P.H. (2006) Regulation of E-cadherin expression by VHL and hypoxia-inducible factor. *Cancer Res.*, **66**, 3567–3575.
37. Barocas,D.A., Rabbani,F., Scherr,D.S. and Vaughan,E.D. Jr (2006) A population-based study of renal cell carcinoma and prostate cancer in the same patients. *BJU Int.*, **97**, 33–36.
38. Pennacchietti,S., Michieli,P., Galluzzo,M., Mazzone,M., Giordano,S. and Comoglio,P.M. (2003) Hypoxia promotes invasive growth by transcriptional activation of the met protooncogene. *Cancer Cell*, **3**, 347–361.

39. Weon,J.L., Yang,S.W. and Potts,P.R. (2018) Cytosolic iron–sulfur assembly is evolutionarily tuned by a cancer-amplified ubiquitin ligase. *Mol. Cell*, **69**, 113–125.
40. Kerkhofs,M., Bittremieux,M., Morciano,G., Giorgi,C., Pinton,P., Parys,J.B. and Bultynck,G. (2018) Emerging molecular mechanisms in chemotherapy: Ca^{2+} signaling at the mitochondria-associated endoplasmic reticulum membranes. *Cell Death Dis.*, **9**, 334.
41. Marchi,S., Lupini,L., Patergnani,S., Rimessi,A., Missiroli,S., Bonora,M., Bononi,A., Corra,F., Giorgi,C., De Marchi,E. *et al.* (2013) Downregulation of the mitochondrial calcium uniporter by cancer-related miR-25. *Curr. Biol.*, **23**, 58–63.
42. Cui,C., Yang,J., Fu,L., Wang,M. and Wang,X. (2019) Progress in understanding mitochondrial calcium uniporter complex-mediated calcium signalling: a potential target for cancer treatment. *Br. J. Pharmacol.*, **176**, 1190–1205.
43. Sugioka-Sugiyama,R. and Sugiyama,T. (2011) Sde2: a novel nuclear protein essential for telomeric silencing and genomic stability in *Schizosaccharomyces pombe*. *Biochem. Biophys. Res. Commun.*, **406**, 444–448.
44. Huang,T.T., Nijman,S.M., Mirchandani,K.D., Galardy,P.J., Cohn,M.A., Haas,W., Gygi,S.P., Ploegh,H.L., Bernards,R. and D'Andrea,A.D. (2006) Regulation of monoubiquitinated PCNA by DUB autocleavage. *Nat. Cell Biol.*, **8**, 339–347.
45. Hui,L. and Chen,Y. (2015) Tumor microenvironment: sanctuary of the devil. *Cancer Lett.*, **368**, 7–13.
46. Ruan,K., Song,G. and Ouyang,G. (2009) Role of hypoxia in the hallmarks of human cancer. *J. Cell. Biochem.*, **107**, 1053–1062.
47. Smith,K.A., Waypa,G.B. and Schumacker,P.T. (2017) Redox signaling during hypoxia in mammalian cells. *Redox Biol.*, **13**, 228–234.
48. Jongen,J.M.J., van der Waals,L.M., Trumpi,K., Laoukili,J., Peters,N.A., Schenning-van Schelven,S.J., Govaert,K.M., Borel Rinkes,I.H.M. and Kranenburg,O. (2017) Downregulation of DNA repair proteins and increased DNA damage in hypoxic colon cancer cells is a therapeutically exploitable vulnerability. *Oncotarget*, **8**, 86296–86311.
49. Fanale,D., Bazan,V., Caruso,S., Castiglia,M., Bronte,G., Rolfo,C., Cicero,G. and Russo,A. (2013) Hypoxia and human genome stability: downregulation of BRCA2 expression in breast cancer cell lines. *Biomed. Res. Int.*, **2013**, 746858.
50. Xiong,Z., Guo,M., Yu,Y., Zhang,F.F., Ge,M.K., Chen,G.Q. and Shen,S.M. (2016) Downregulation of AIF by HIF-1 contributes to hypoxia-induced epithelial–mesenchymal transition of colon cancer. *Carcinogenesis*, **37**, 1079–1088.
51. Sethumadhavan,S., Silva,M., Philbrook,P., Nguyen,T., Hatfield,S.M., Ohta,A. and Sitkovsky,M.V. (2017) Hypoxia and hypoxia-inducible factor (HIF) downregulate antigen-presenting MHC class I molecules limiting tumor cell recognition by T cells. *PLoS One*, **12**, e0187314.
52. Iglesias-Gato,D., Wikstrom,P., Tyanova,S., Lavallee,C., Thysell,E., Carlsson,J., Hagglof,C., Cox,J., Andren,O., Stattin,P. *et al.* (2016) The proteome of primary prostate cancer. *Eur. Urol.*, **69**, 942–952.
53. umareswaran,R., Ludkovski,O., Meng,A., Sykes,J., Pintilie,M. and Bristow,R.G. (2012) Chronic hypoxia compromises repair of DNA double-strand breaks to drive genetic instability. *J. Cell Sci.*, **125**, 189–199.
54. Perez-Riverol,Y., Csordas,A., Bai,J., Bernal-Llinares,M., Hewapathirana,S., Kundu,D.J., Inuganti,A., Griss,J., Mayer,G., Eisenacher,M. *et al.* (2019) The PRIDE database and related tools and resources in 2019: improving support for quantification data. *Nucleic Acids Res.*, **47**, D442–D450.